coatings

MDPI

Article

Fully Inkjet-Printed Short-Channel Metal-Oxide Thin-Film Transistors Based on Semitransparent ITO/Au Source/Drain Electrodes

Yuzhi Li and Shengdong Zhang *

School of Electronic and Computer Engineering, Peking University Shenzhen Graduate School, Shenzhen 518055, China; liyuzhi1991@gmail.com

* Correspondence: zhangsd@pku.edu.cn

Received: 5 September 2020; Accepted: 28 September 2020; Published: 30 September 2020

Abstract: In this work, short-channel semitransparent indium-tin-oxide (ITO)/Au electrode pairs were fabricated via inkjet printing and lift-off technology. The printed hydrophobic coffee stripes not only define the channel length of ITO/Au electrode pairs, but also help the realization of uniform short-channel $In_{0.95}Ga_{0.05}O_x$ thin-film transistors (TFTs). The patterned semitransparent ITO/Au films, with the assistance of inkjet printing, exhibit an excellent conductivity compared to that of printed ITO films, and the short-channel $In_{0.95}Ga_{0.05}O_x$ TFTs based on the semitransparent ITO/Au source/drain electrodes exhibit a maximum mobility of 2.9 $cm^2\ V^{-1}\ s^{-1}$. This work proposes a method to prepare patterned high-conductive electrodes for TFTs with the assistance of inkjet printing.

Keywords: inkjet printing; semitransparent electrodes; short channel; thin-film transistors

1. Introduction

Metal-oxide thin-film transistors (MO-TFTs) have received much attention for their extensive application prospects in large-area electronics. In contrast to amorphous silicon (a-Si) TFTs, MO-TFTs exhibit excellent characteristics, including a relatively high mobility, good uniformity, mechanical stress tolerance, and a high transparency for visible light, showing their great potential to be applied in flexible and large-area displays [1,2]. More recently, to lower the fabrication cost, much attention is focused on the development of low-temperature, solution-processed MO-TFTs [3,4]. Inkjet printing, as a cost-effective, noncontact, and directly patternable solution-based processing technique, is attractive in the production of MO-TFTs. Over the past decade, researchers have made constant attempts to fabricate MO-TFTs via inkjet printing, but it is still difficult to directly print uniform MO-TFTs [5–7].

To date, most of the reports on inkjet-printed MO TFTs are only focused on the semiconductor layers and demonstrated that the electrical performance of printed oxide semiconductors is comparable with the one based on other solution processing methods such as spin coating [8–10]. Besides, there are some reports on printing source/drain (S/D) electrodes for MO-TFTs. The ideal materials of S/D electrodes applied for MO-TFTs require good conductivity and low-resistance contact to channel layers. Hong et al. [11] reported that oleic acid-capped Ag nanoparticles as S/D in MO-TFTs improve the field-effect mobility, which was ascribed to the effective suppression of the significant Ag migration. However, the existence of organic species between the Ag electrodes and oxide semiconductor may play a tarp role, which is bad for the electrical performance of the TFTs. Scheideler et al. [12] showed the high performance, aqueous-printed InO_x TFTs with printed aluminum-doped cadmium oxide (ACO) S/D electrodes. However, the intrinsic toxicity of ACO makes it a nonideal candidate for transparent conducting materials. For the MO-TFTs based on the vacuum process, indium-tin-oxide (ITO) is an ideal material for S/D electrodes because of its acceptable electrical conductivity and ohmic contact

with the oxide semiconducting layer [13,14]. Printed ITO as S/D electrodes integrated in MO-TFTs have also been reported, but the conductive films exhibit inferior electrical conductivity compared with those based on vacuum techniques [15,16]. Therefore, it is necessary to seek a feasible way to improve the conductivity of printed MO conductors.

The channel length is a critical parameter that determines the device density and the operation speed of the devices. The transition frequency f_T, an important quantity to evaluate the speed of TFT, is defined as [17]

$$f_T = \frac{\mu_e(V_{GS}-V_{th})}{4\pi L^2}\frac{C_{ch}}{C_{ch}+C_p} \quad (1)$$

where μ_e is the field-effect mobility, C_{ch} is the channel capacitance, and C_p is the parasitic capacitance. According to the equation, the response speed of TFTs is inversely proportional to the square of the channel length (L). Thus, the operating speed of TFTs can be improved by decreasing the channel length. Nowadays, the channel length of TFTs in the flat panel displays (FPDs) is generally less than 10 μm. However, it is difficult to directly print uniform S/D electrodes with such a small-scale channel length using a common inkjet printer for the positional inaccuracy and the influence of the surrounding environment [18].

In this work, we demonstrate uniform short-channel $In_{0.95}Ga_{0.05}O_x$ TFTs via inkjet printing. The ITO/Au conductive film patterned via inkjet printing and lift-off technology, which showed excellent electrical conductivity, was utilized for S/D electrodes. The hydrophobic coffee stripes prepared by solvent etching were utilized to define short-channel ITO/Au electrode pairs and fabricate the $In_{0.95}Ga_{0.05}O_x$ TFTs. The semitransparent ITO/Au electrode pairs exhibit an average channel length of less than 2 μm. The $In_{0.95}Ga_{0.05}O_x$ TFTs based on the semitransparent ITO/Au S/D electrodes showed a maximum mobility of 2.9 $cm^2\ V^{-1}\ s^{-1}$ and an I_{on}/I_{off} ratio of bigger than 10^6.

2. Experiment

2.1. Solution and Inks Preparation

CTL-107MK solute and CT-SOLV180 solvent were mixed with a volume ratio of 1:10 to prepare Cytop solution. Methoxyethanol and ethylene glycol were mixed with a volume ratio of 1:1 to prepare the solvent mixture for ITO and $In_{0.95}Ga_{0.05}O_x$ precursor ink. The total concentration of ITO ink is 0.5 M with a Sn/(In + Sn) molar ratio of 5%, while the concentration of $In_{0.95}Ga_{0.05}O_x$ ink is 0.2 M with a Ga/(In+Ga) molar ratio of 5%. The $Al_{0.5}Zr_{0.5}O_x$ precursor ink (0.4 M) was synthesized by dissolving $ZrO(NO_3)_2{\cdot}xH_2O$ and $Al(NO_3)_3{\cdot}xH_2O$ into deionized water. All of the solution and inks were stirred at room temperature for 12 h and filtered through a 0.22 μm syringe filter before use.

2.2. Fabrication of Short-Channel ITO/Au Electrode Pairs

The short-channel ITO/Au electrode pairs patterned via inkjet printing and lift-off technology are shown in Figure 1. Firstly, a 10 nm-thick Au layer was deposited on glass using thermal evaporation (Figure 1a). Then, the ultrathin Cytop layer was spin-coated on the Au film with a rotation speed of 4000 rpm (Figure 1b). Next, the Cytop layer was etched by printing pure Cytop solvent using an inkjet printer (DMP-2800), and narrow stripes formed due to the coffee-ring effect (Figure 1c). After the sample was annealed at 120 °C in air condition for 10 min, an additional Cytop layer was deposited on the sample based on the same processes (Figure 1d). Subsequently, the narrow stripes, which were perpendicular to the pre-produced stripes, were obtained by etching the Cytop layer (Figure 1e). After that, the undesired residual of Cytop between stripes was removed by oxygen plasma treatment (Figure 1f), and the wettability of the Au film was improved by UV irradiation. Next, the ITO precursor ink was selectively printed onto the hydrophobic stripe patterns to prepare isolated precursor islands (Figure 1g). After that, the sample was annealed at 350 °C for 1 h in air. To pattern the ITO/Au film for short-channel ITO/Au electrode pairs (Figure 1h), the sample was sonicated in deionized water for 10 min.

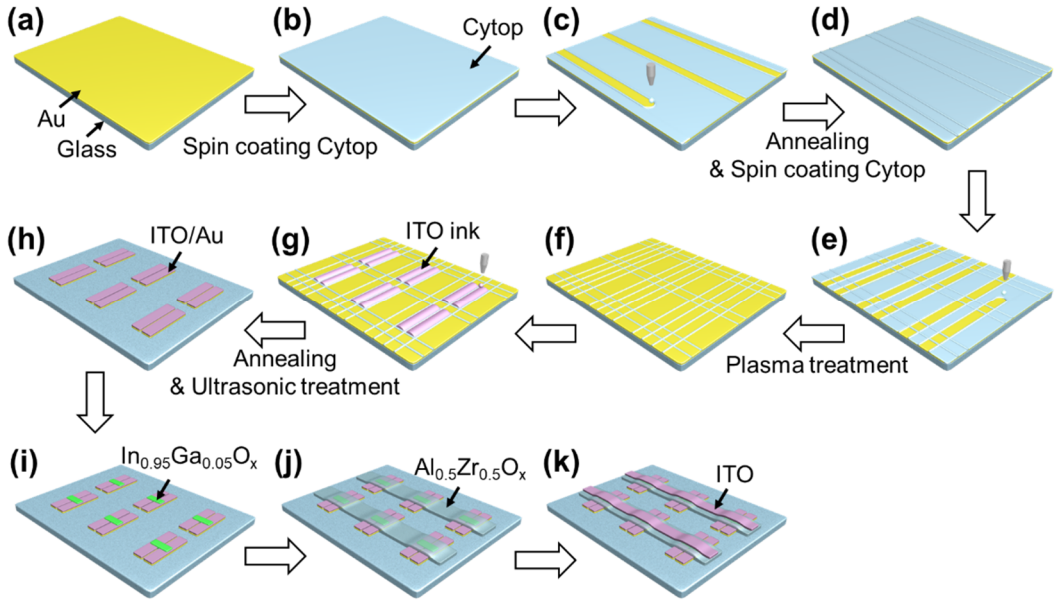

Figure 1. (**a**) Ultrathin Au layer deposited on glass substrate; (**b**) Cytop layer deposited on Au film; (**c**) Hydrophobic coffee stripes formed by solvent etching; (**d**) Second Cytop layer deposited on the substrate; (**e**) Perpendicular hydrophobic coffee stripes formed by solvent etching; (**f**) Hydrophobic stripe patterns on Au film; (**g**) Selectively printing indium-tin-oxide (ITO) ink on hydrophobic stripe patterns; (**h**) Short-channel ITO/Au electrode pairs on glass substrate; (**i**) Printed $In_{0.95}Ga_{0.05}O_x$ semiconductor films on short-channel ITO/Au electrode pairs; (**j**) Printed $Al_{0.5}Zr_{0.5}O_x$ films as dielectric layer; (**k**) Printed ITO films as gate electrodes.

2.3. Devices Fabrication

Herein, a top-gate, bottom-contact structure was employed to produce $In_{0.95}Ga_{0.05}O_x$ TFTs via inkjet printing. The short-channel ITO/Au S/D electrodes were prepared as described above, and fabrication processes of other functional layers, including the semiconductor layer, the dielectric layer, and the gate electrode, were performed following previous work [19]. Briefly, the ultrathin Cytop layer was spin-coated on the sample with a rotation speed of 4000 rpm (40 s). Then, Cytop solvent was printed to etch the Cytop layer and forms hydrophobic stripe patterns. After that, the undesired residual of Cytop between stripes was removed by oxygen plasma treatment, and the wettability of the substrate was improved by UV irradiation. Next, the oxide precursor ink was printed onto the hydrophobic stripe patterns and then annealed at a certain temperature to form the functional layer. As shown in Figure 1i, $In_{0.95}Ga_{0.05}O_x$ semiconductor films with a width of ~50 μm and a thickness of ~11 nm were printed on the short-channel ITO/Au electrode pairs. Next, the $Al_{0.5}Zr_{0.5}O_x$ dielectric films with a width of ~120 μm and a thickness of ~120 nm were printed to fully cover the semiconductor layer (Figure 1j). Finally, ITO films with a width of ~75 μm and a thickness of ~45 nm were printed as gate electrodes (Figure 1k).

2.4. Characterization

The thickness of film was characterized by a surface profiler (Veeco Instruments Inc., New York, NY, USA). Optical transmission spectra of thin films were measured by a UV–2600 spectrophotometer (Shimadzu, Tokyo, Japan). The surface morphologies of prepared films were measured using an atomic force microscope (AFM, Bruker, Multimode 8, Madison, WI, USA). Polarizing microscope images were characterized using an optical microscope (Nikon Eclipse E600 POL, New York, NY, USA). A semiconductor parameter analyzer (Keithley 4200-SCS, Cleveland, OH, USA) was employed to characterize the electrical properties of printed TFTs in air condition. A contact angle analyzer

(Biolin Scientific, Theta Lite 101, Gothenburg, Sweden) was employed to measure the surface tension of inks. The mobility (μ) and subthreshold slope (*SS*) of TFTs were calculated using the following equations:

$$I_{DS} = \frac{W\mu C_i}{2L}(V_{GS}-V_{th})^2 \quad (2)$$

$$SS = \frac{\partial V_{GS}}{\partial \log(I_{DS})} \quad (3)$$

where C_i is the areal capacitance, V_{th} is the threshold voltage, W and L correspond to the channel width and length, respectively.

3. Results and Discussion

Figure 2 shows the optical transmittance of the prepared Au film and ITO/Au film. It was found that both of the Au and ITO/Au films are semitransparent, and the transmittance at the visible-light wavelengths (400−700 nm) increased after the single layer of Au was covered by ITO layer. It means that both of the parasitic absorption and the reflectance in the whole visible wavelength range are reduced, because the interference of the incident light at the interfaces was destroyed [20]. The sheet resistance of 10 nm-thick Au film is ~12.0 Ω/square and the calculated resistivity is ~1.2×10^{-5} Ω·cm, which is about an order of magnitude higher than that of bulk film (2.44×10^{-6} Ω·cm). The higher resistivity of the ultrathin Au film was ascribed to the existence of nano holes, resulting from the island growth mode of the film [21,22]. The ITO/Au film with a thickness of ~40 nm exhibits a sheet resistance of ~9.8 Ω/square and the resistivity is ~3.9×10^{-5} Ω·cm. The increase in resistivity of ITO/Au composite electrodes is due to the relatively high resistivity of the printed ITO film (~2.4×10^{-1} Ω·cm) annealed at 350 °C. Interestingly, the single layer of 10 nm-thick Au annealed at 350 °C shows infinite resistance, and it can be removed by ultrasonic treatment in deionized water, whereas the film without annealing still adheres to glass substrates under the same treatment.

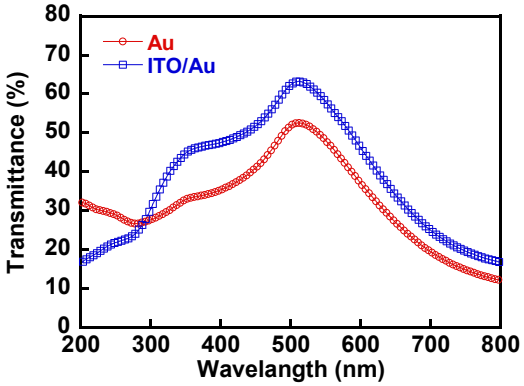

Figure 2. Optical transmission spectra of the Au film and ITO/Au film.

Figure 3a,b shows the AFM images of Au films without and with annealing, respectively. The surface root mean square (RMS) value of Au film without annealing is 1.62 nm, while that of the annealed Au film is 17.4 nm. The overlapped nanoscale Au particles (average particle size of ~40 nm) grow into isolated sub-microscale Au particles (average particle size of ~350 nm) after annealing, which leads to the great increase in the RMS value and infinite resistance of the Au film. Thanks to the relatively large gap between the isolated sub-microscale Au particles, the water will fill the gap during ultrasonic treatment. As a result, the sub-microscale Au particles can be easily stripped from the substrate with the help of cavitation bubble collapse under ultrasonic bath [23]. Figure 3c shows the microscope image of prepared short-channel ITO/Au electrode pairs, while Figure 3d shows an enlarged image of a pair of electrode with a channel length of 1.67 μm. The average channel length

measured from 12 pairs of electrodes is ~1.82 µm. It can be clearly seen that the region of the Au layer uncovered by ITO was thoroughly removed and the patterned ITO/Au films have smooth boundaries as well as uniform channel length. It suggests that the ITO layer can prevent the water from permeating into the Au layer and thus protecting the Au layer covered by the ITO layer from being lifted off. The current versus voltage plot (Figure 3e) collected from the ITO/Au electrode pair exhibits a current level of 1×10^{-12} A, indicating that the short-channel electrode pairs are electrically isolated.

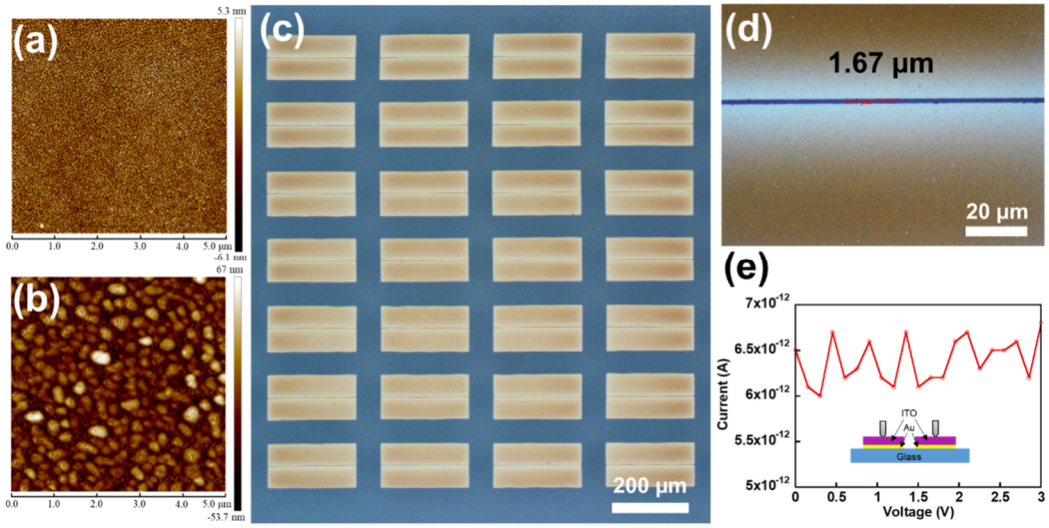

Figure 3. Atomic force microscope (AFM) images (5 µm × 5 µm) of Au films (**a**) without and (**b**) with annealing at 350 °C. (**c**) Polarizing microscope image of prepared short-channel ITO/Au electrode pairs and (**d**) enlarged image in channel region of a pair of electrodes. (**e**) Plot of current versus voltage collected from ITO/Au electrode pair.

Pure aqueous inks are more favorable for printing oxide dielectric compared to organic inks, because the printed oxide dielectric films prepared using aqueous ink are generally free of nanopores and carbon impurities. However, the relatively low viscosity of aqueous inks leads to difficulties in the regulation of the spreading and pinning of the droplet. Hydrophobic coffee patterns are employed here to control the spreading of aqueous inks. Interestingly, as shown in Figure 4, the different aqueous oxide precursor deposited on the hydrophobic stripe patterns exhibits different pinning behavior. The deposited AlO_x and $Al_{0.5}Zr_{0.5}O_x$ precursor inks can well pin on the inner periphery of a coffee stripe, whereas deposited ZrO_x precursor ink shows unpinning behavior on one side of a coffee stripe and forms nonuniform patterns. The different behavior of the aqueous inks is associated with the interaction between metal cations and the water molecules. As shown in Figure 4d, the surface tension of AlO_x precursor ink (aqueous $Al(NO_3)_3$) increases with an increasing solute concentration, which is associated with the formation of Al^{3+} complexes (Al^{3+}–nH_2O). The strength of the interaction between Al^{3+} and H_2O is higher than that between water molecules. However, the surface tension of ZrO_x precursor ink shows a decreasing trend with an increasing solute concentration, indicating that $[ZrO]^{2+}$ has a lower binding strength with water molecules comparing with that of the neighboring water molecules. Accordingly, the unpinning behavior of the ZrO_x precursor ink is ascribed to a relatively low binding strength of $[ZrO]^{2+}$ with the hydroxyl group (–OH) grown on the glass substrate. Due to the existence of Al^{3+} in the $Al_{0.5}Zr_{0.5}O_x$ precursor ink, the deposited $Al_{0.5}Zr_{0.5}O_x$ precursor films exhibit well-defined patterns on the deposited AlO_x precursor films. Herein, $Al_{0.5}Zr_{0.5}O_x$ was employed as the dielectric material to fabricate short-channel $In_{0.95}Ga_{0.05}O_x$ TFTs.

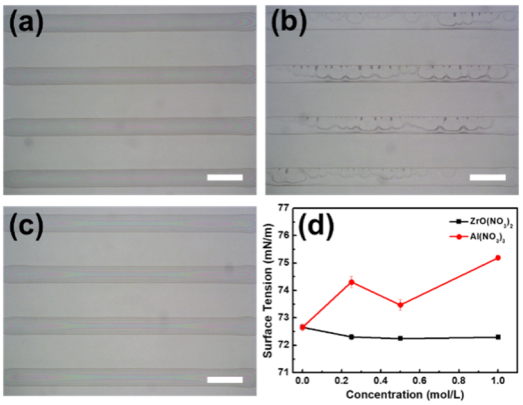

Figure 4. Polarizing microscope images of printed (**a**) AlO_x precursor film, (**b**) ZrO_x precursor film and (**c**) $Al_{0.5}Zr_{0.5}O_x$ precursor film (bar = 300 μm). (**d**) Surface tension versus concentration for aqueous $Al(NO_3)_3$ and $ZrO(NO_3)_2$ inks.

To characterize the dielectric properties of the printed $Al_{0.5}Zr_{0.5}O_x$ films, capacitors based on the 120 nm-thick $Al_{0.5}Zr_{0.5}O_x$ dielectric films were fabricated. Figure 5 shows leakage current as a function of electric fields, while the inset presents areal capacitance versus frequency. The capacitor exhibits acceptable dielectric properties with a high breakdown electric field (>7 MV cm^{-1}), and a low leakage current density ~10^{-6} A cm^{-2} at 2 MV cm^{-1}. The areal capacitance at 1 kHz is ~220 nF cm^{-2}, and the calculated dielectric constant is ~11, which is higher than the value of solution-processed AlO_x films, but smaller than that of solution-processed ZrO_x films [24,25]. The frequency dependence of areal capacitance is ascribed to the hydroxyl groups in printed $Al_{0.5}Zr_{0.5}O_x$ film. The orientation polarization of hydroxyl groups is in the range of 10^{-9} to 10^{-5} s, approximately [26]. As a result, the hydroxyl groups gradually fail to respond with external high-frequency signals, inducing the frequency-dependent capacitance of printed $Al_{0.5}Zr_{0.5}O_x$ films.

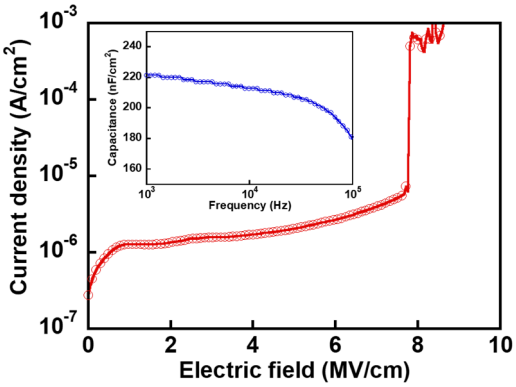

Figure 5. Leakage current density and areal capacitance characteristics of the printed $Al_{0.5}Zr_{0.5}O_x$ dielectric films.

Figure 6a shows microscope image of printed short-channel $In_{0.95}Ga_{0.05}O_x$ TFTs. The good uniformity of each TFT in the array indicates that the nonuniform deposition of films induced by the interaction of adjacent droplet islands was eliminated, which is associated with the effective limitation of the ink spreading by the hydrophobic coffee stripes. Figure 6b shows the typical output curve of the short-channel TFT, while Figure 6c shows the corresponding transfer curve. There is no current crowding effect at the low V_{DS} region in the output curve, indicating good ohmic contact between the ITO/Au S/D electrodes and the $In_{0.95}Ga_{0.05}O_x$ channel layer. The transfer curve exhibits little clockwise hysteresis, indicating that some of the accumulated electrons are trapped in the dielectric/channel interface [25,27], which is associated with the relatively high thickness of the $Al_{0.5}Zr_{0.5}O_x$ films (~120 nm). The mobility

extracted from the transfer curves of 12 devices is in the range of 2.2 ± 0.7 cm^2 V^{-1} s^{-1}, and the I_{on}/I_{off} ratio of the devices is larger than 10^6. These results indicate that the application of the short-channel semitransparent ITO/Au electrode pairs in the oxide TFTs is feasible.

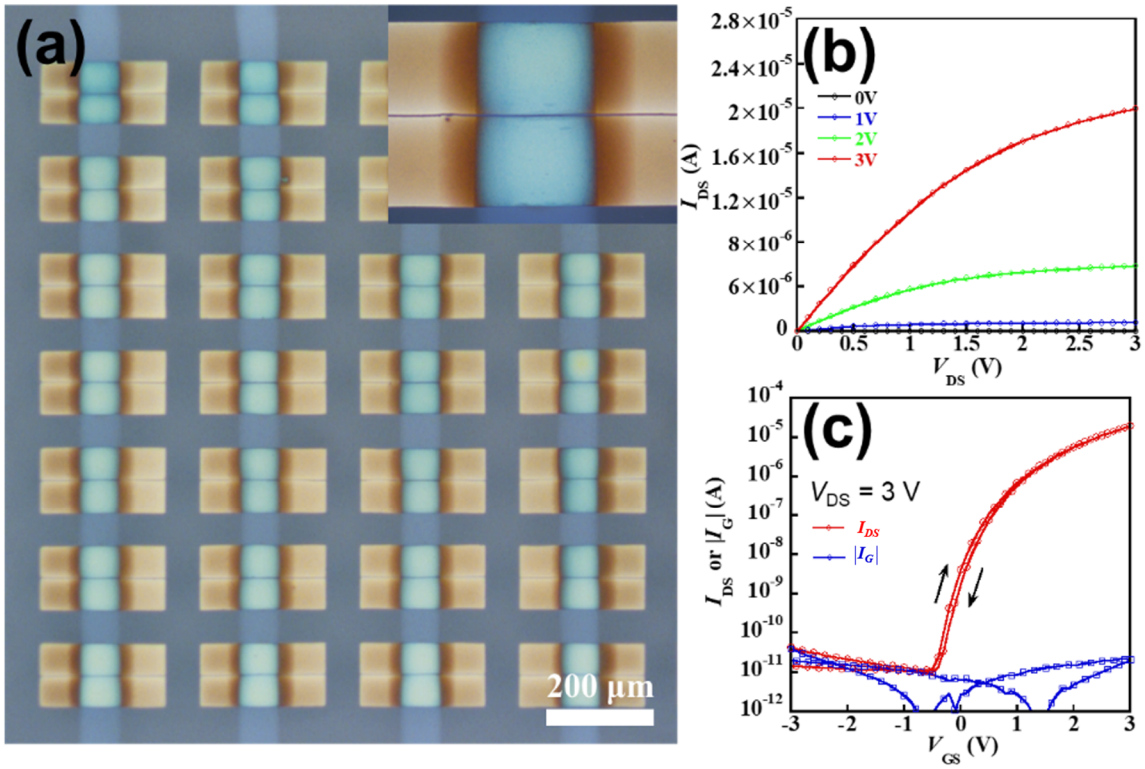

Figure 6. (**a**) Polarizing microscope image of printed short-channel $In_{0.95}Ga_{0.05}O_x$ thin-film transistors (TFTs). The inset is a close-up image of one printed TFT. Typical (**b**) output and (**c**) transfer curves of the printed TFT.

4. Conclusions

In summary, inkjet-printed short-channel $In_{0.95}Ga_{0.05}O_x$ TFTs based on semitransparent ITO/Au S/D electrodes were demonstrated. The semitransparent ITO/Au stacked films exhibits an excellent electrical conductivity (~1.2×10^{-5} Ω·cm) compared with that of printed ITO films (~2.4×10^{-1} Ω·cm). With the help of hydrophobic coffee stripes, the short-channel semitransparent ITO/Au electrodes pairs were fabricated with an average channel length of less than 2 μm, and the uniform top-gate $In_{0.95}Ga_{0.05}O_x$ TFTs were also fabricated based on the short-channel ITO/Au electrodes pairs. The $In_{0.95}Ga_{0.05}O_x$ TFTs exhibits a maximum mobility of 2.9 cm^2 V^{-1} s^{-1} and an I_{on}/I_{off} ratio of large than 10^6. This work proposes a method to prepare patterned high-conductive electrodes for TFTs with the assistance of inkjet printing.

Author Contributions: Conceptualization, Y.L. and S.Z.; Formal analysis, Y.L.; Funding acquisition, S.Z.; Writing—original draft, Y.L.; Writing—review and editing, S.Z. All authors have read and agreed to the published version of the manuscript.

Funding: This work was supported by the National Natural Science Foundation of China (Grant No. 61774010) and the Shenzhen Municipal Scientific Program (Grant No. JCYJ20180504165449640).

Acknowledgments: The authors thank Linfeng Lan for his great support.

Conflicts of Interest: The authors declare no conflict of interest.

References

1. Petti, L.; Münzenrieder, N.; Vogt, C.; Faber, H.; Büthe, L.; Cantarella, G.; Bottacchi, F.; Anthopoulos, T.D.; Tröster, G. Metal oxide semiconductor thin-film transistors for flexible electronics. *Appl. Phys. Rev.* **2016**, *3*, 021303. [CrossRef]
2. Nomura, K.; Ohta, H.; Takagi, A.; Kamiya, T.; Hirano, M.; Hosono, H. Room-temperature fabrication of transparent flexible thin-film transistors using amorphous oxide semiconductors. *Nature* **2004**, *432*, 488–492. [CrossRef] [PubMed]
3. Wang, B.; Huang, W.; Chi, L.; Al-Hashimi, M.; Marks, T.J.; Facchetti, A. High-*k* gate dielectrics for emerging flexible and stretchable electronics. *Chem. Rev.* **2018**, *118*, 5690–5754. [CrossRef] [PubMed]
4. Liu, A.; Zhu, H.; Sun, H.; Xu, Y.; Noh, Y. Solution processed metal oxide high-*k* dielectrics for emerging transistors and circuits. *Adv. Mater.* **2018**, *30*, 1706364. [CrossRef]
5. Garlapati, S.K.; Divya, M.; Breitung, B.; Kruk, R.; Hahn, H.; Dasgupta, S. Printed electronics based on inorganic semiconductors: From processes and materials to devices. *Adv. Mater.* **2018**, *30*, 1707600. [CrossRef]
6. Chung, S.; Cho, K.; Lee, T. Recent progress in inkjet-printed thin-film transistors. *Adv. Sci.* **2019**, *6*, 1801445. [CrossRef]
7. Shao, F.; Wan, Q. Recent progress on jet printing of oxide-based thin film transistors. *J. Phys. D* **2019**, *52*, 143002. [CrossRef]
8. Wu, S.; Zhang, Q.; Chen, Z.; Mo, L.; Shao, S.; Cui, Z. Inkjet printing of oxide thin film transistor arrays with small spacing with polymer-doped metal nitrate aqueous ink. *J. Mater. Chem. C* **2017**, *5*, 7495–7503. [CrossRef]
9. Avis, C.; Hwang, H.R.; Jang, J. Effect of channel layer thickness on the performance of indium-zinc-tin oxide thin film transistors manufactured by inkjet printing. *ACS Appl. Mater. Interfaces* **2014**, *6*, 10941–10945. [CrossRef]
10. Lee, J.S.; Kwack, Y.; Choi, W. Inkjet-printed In_2O_3 thin-film transistor below 200 °C. *ACS Appl. Mater. Interfaces* **2013**, *5*, 11578–11583. [CrossRef]
11. Hong, G.R.; Lee, S.S.; Park, H.J.; Jo, Y.; Kim, J.Y.; Lee, H.S.; Kang, Y.C.; Ryu, B.; Song, A.; Chung, K.; et al. Unraveling the issue of Ag migration in printable source/drain electrodes compatible with versatile solution-processed oxide semiconductors for printed thin-film transistor applications. *ACS Appl. Mater. Interfaces* **2017**, *9*, 14058–14066. [CrossRef]
12. Scheideler, W.J.; Kumar, R.; Zeumault, A.R.; Subramanian, V. Low-temperature-processed printed metal oxide transistors based on pure aqueous inks. *Adv. Funct. Mater.* **2017**, *27*, 1606062. [CrossRef]
13. Jang, J.; Kitsomboonloha, R.; Swisher, S.L.; Park, E.S.; Kang, H.; Subramanian, V. Transparent high-performance thin film transistors from solution-processed SnO. *Adv. Mater.* **2013**, *25*, 1042–1047. [CrossRef] [PubMed]
14. Hennek, J.W.; Xia, Y.; Everaerts, K.; Hersam, M.C.; Facchetti, A.; Marks, T.J. Reduced contact resistance in inkjet printed high-performance amorphous indium gallium zinc oxide transistors. *ACS Appl. Mater. Interfaces* **2012**, *4*, 1614–1619. [CrossRef] [PubMed]
15. Li, Y.; He, P.; Chen, S.; Lan, L.; Dai, X.; Peng, J. Inkjet-printed oxide thin-film transistors based on nanopore-free aqueous-processed dielectric for active-matrix quantum-dot light-emitting diode displays. *ACS Appl. Mater. Interfaces* **2019**, *11*, 28052–28059. [CrossRef]
16. Li, Y.; Lan, L.; Hu, S.; Gao, P.; Dai, X.; He, P.; Li, X.; Peng, J. Fully printed top-gate metal-oxide thin-film transistors based on scandium-zirconium-oxide dielectric. *IEEE Trans. Electron Devices* **2019**, *66*, 445–450. [CrossRef]
17. Klauk, H. Organic thin-film transistors. *Chem. Soc. Rev.* **2010**, *39*, 2643. [CrossRef]
18. Ning, H.; Tao, R.; Fang, Z.; Cai, W.; Chen, J.; Zhou, Y.; Zhu, Z.; Zheng, Z.; Yao, R.; Xu, M.; et al. Direct patterning of silver electrodes with 2.4 μm channel length by piezoelectric inkjet printing. *J. Colloid Interface Sci.* **2017**, *487*, 68–72. [CrossRef]
19. Li, Y.; Lan, L.; Sun, S.; Lin, Z.; Gao, P.; Song, W.; Song, E.; Zhang, P.; Peng, J. All inkjet-printed metal-oxide thin-film transistor array with good stability and uniformity using surface-energy patterns. *ACS Appl. Mater. Interfaces* **2017**, *9*, 8194–8200. [CrossRef]
20. Yu, S.; Li, L.; Lyu, X.; Zhang, W. Preparation and investigation of nano-thick FTO/Ag/FTO multilayer transparent electrodes with high figure of merit. *Sci. Rep.* **2016**, *6*, 20399. [CrossRef]

21. Zeng, Y.; Ning, H.; Zheng, Z.; Zhang, H.; Fang, Z.; Yao, R.; Xu, M.; Wang, L.; Lan, L.; Peng, J.; et al. Island-like AZO/Al_2O_3 bilayer channel structure for thin film transistors. *Adv. Mater. Interfaces* **2017**, *4*, 1700063. [CrossRef]
22. Martin, L.W.; Chu, Y.H.; Ramesh, R. Advances in the growth and characterization of magnetic, ferroelectric, and multiferroic oxide thin films. *Mater. Sci. Eng. R* **2010**, *68*, 89–133. [CrossRef]
23. Deng, C.; Gao, P.; Lan, L.; He, P.; Zhao, X.; Zheng, W.; Chen, W.; Zhong, X.; Wu, Y.; Liu, L.; et al. Ultrasensitive and highly stretchable multifunctional strain sensors with timbre-recognition ability based on vertical graphene. *Adv. Funct. Mater.* **2019**, *29*, 1907151. [CrossRef]
24. Jo, J.; Kim, J.; Kim, K.; Kang, J.; Kim, M.; Kim, K.; Ko, H.; Kim, Y.; Park, S.K. Highly stable and imperceptible electronics utilizing photoactivated heterogeneous sol-gel metal-oxide dielectrics and semiconductors. *Adv. Mater.* **2015**, *27*, 1182–1188. [CrossRef] [PubMed]
25. Park, J.H.; Yoo, Y.B.; Lee, K.H.; Jang, W.S.; Oh, J.Y.; Chae, S.S.; Baik, H.K. Low-temperature, high-performance solution-processed thin-film transistors with peroxo-zirconium oxide dielectric. *ACS Appl. Mater. Interfaces* **2013**, *5*, 410–417. [CrossRef]
26. Wang, H.; Xu, W.; Zhou, S.; Xie, F.; Xiao, Y.; Ye, L.; Chen, J.; Xu, J. Oxygen plasma assisted high performance solution-processed Al_2O_x gate insulator for combustion-processed $InGaZnO_x$ thin film transistors. *J. Appl. Phys.* ***2015***, 117, *035703. [.org/10.1063/1.4906107*CrossRef]
27. Egginger, M.; Bauer, S.; Schwödiauer, R.; Neugebauer, H.; Sariciftci, N.S. Current versus gate voltage hysteresis in organic field effect transistors. *Chem. Mon.* **2009**, *140*, 735–750. [CrossRef]